A Hi-C map of the senescent genome at kilobase resolution reveals novel associations between chromatin changes and gene expression

Computational Biology Senior Thesis

Kelly Clark

First Reader: Dr. Nicola Neretti

Second Reader: Dr. Ritambhara Singh

Introduction

Understanding aging is crucial to improving human health, and a contributor to aging is Cellular Senescence (CS), a state of irreversible cell cycle arrest [15]. CS exacerbates aging through the secretion of proteins that regulate inflammation, including interferons (IFN) and interleukins (IL), called the Senescence Associated Secretory Phenotype (SASP). Senescent cells accumulate with the progression of age and are thus implicated in contributing to age-associated diseases through SASP [5]. The senescence phenotype can be induced in multiple ways. The first observed was replicative senescence (RS), in which cells are passaged to telomeric exhaustion [15]. It can also result from activation of an oncogene such as Ras in oncogene induced senescence (OIS), or from DNA damage in DNA damage induced senescence (DDIS) [20].

Senescent cells show changes in the nucleus when compared to proliferating cells such as chromatin remodeling. This includes the formation of senescence-associated heterochromatin foci (SAHF) in OIS [17, 20], senescence-associated distention of satellites (SADS) [24], histone depletion, heterochromatin loss, dissociation of chromatin from the nuclear lamina [23], and increased accessibility of lamin associated domains (LADs) [11].

Chromatin conformation capture technologies include 3C, 4C, 5C, ChIA-PET, and Hi-C and can be used to investigate the three-dimensional organization of chromatin [1, 11, 19, 23]. Hi-C in particular can be used to create heatmaps of the contacts between loci across the entire genome. These heatmaps demonstrate first chromosome territories, in which each chromosome has more contacts with itself than with other chromosomes (Fig. 1a). At low resolutions, two compartments, A and B, are visible on these heatmaps with more intra-compartment than inter-compartment contacts (Fig. 1b). Compartment A is more active and gene-dense, while compartment B is more heterochromatic. At higher resolutions, these can be split into subcompartments A1-A2 and B1-B4, each characterized by a dif-

ferent enrichment for particular chromatin marks, lamin associated domains, and nucleolus associated domains..

Also at high resolutions, topologically associating domains (TADs) and chromatin loops can be identified (Fig. 1c-d), with TADs being areas of 40 kilobases to 3 megabases with more contacts within the region than to other regions, and loops being two loci with increased contacts relative to the surrounding region [19]. Loops have been associated with contacts to enhancers and promoters and thus are a possible means of gene regulation. In three dimensions, loops have two anchor points, the regions of increased contacts which are often anchored by CTCF, with the chromatin between them extruded, forming the loop [19].

Many TAD callers have been developed, each with its strengths and weaknesses. These callers take a variety of approaches, including linear scoring, clustering, statistical modeling, and use of network features. Some call TADs with gaps between and some without. Some call disjoint TADs, while others call nested and overlapping TADs. Because there is no true set of TADs against which to compare the performance of TAD callers, callers must be compared against each other for assessment. Further, the TAD boundaries called may not line up with compartment boundaries called separately [28].

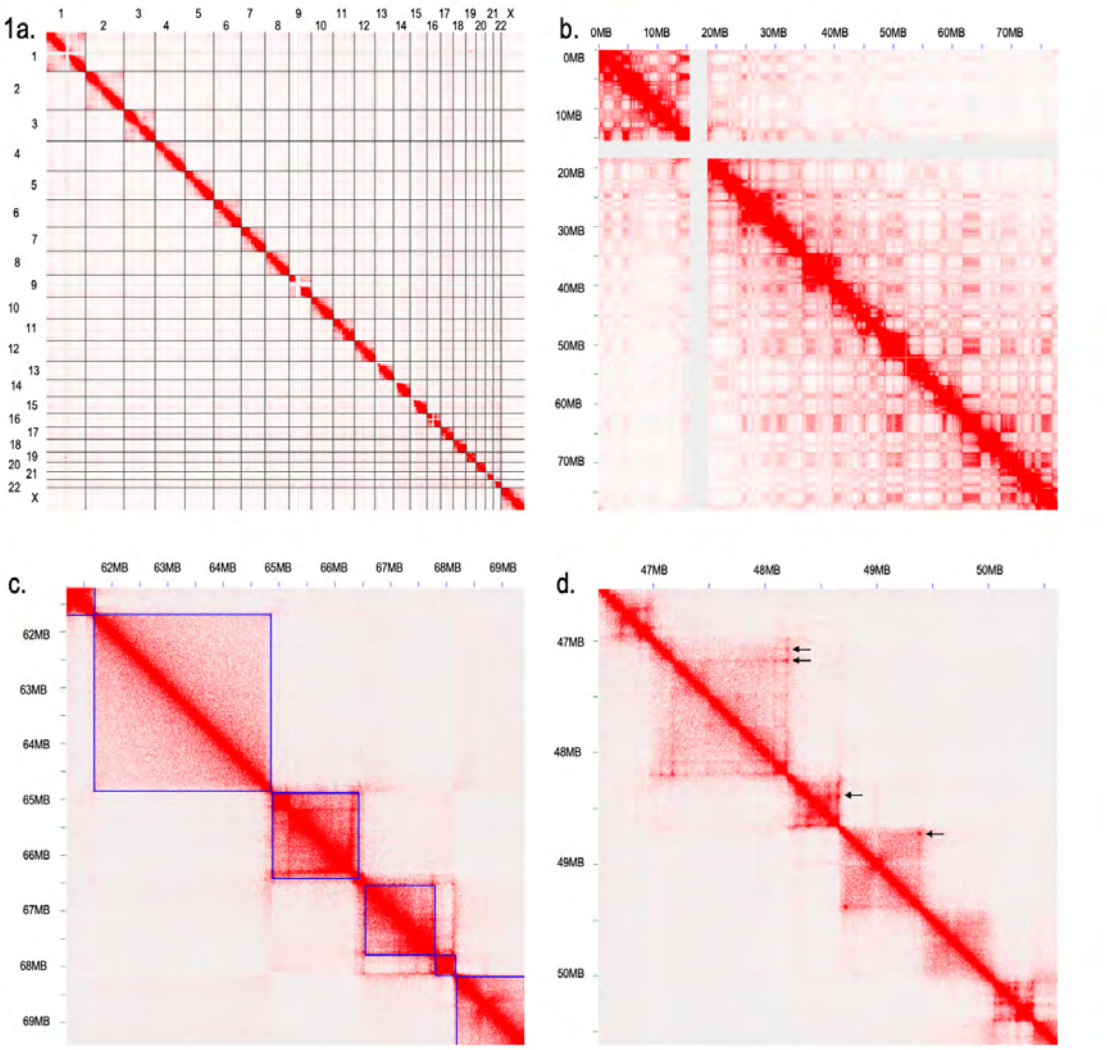

Figure 1. Hi-C data shows genome organization at multiple levels. At the lowest resolutions, contacts are concentrated into chromosome territories (a, chromosomes labeled on axes). Within intra-chromosomal heatmaps, the checkerboard pattern delineates compartments (b). TADs are visible as regions of increased contacts at a higher resolution (c), and loops can be identified as points of enriched contacts between two loci compared to the surrounding area (d). Heatmaps are shown for proliferating LF1 cells.

Between proliferating and senescent states, compartments have been observed to switch from A to B and B to A, though B to A switches occur more often [16]. On the domain scale, TADs switch between compartments during senescence [7]. Here, we call TADs, loops, subcompartments, and compartments for our 3 kilobase resolution Hi-C maps of proliferating and senescent lung fibroblasts to investigate in high resolution the changes to genome organization in RS on a global scale, and we identify regions relevant to senescence, including cell cycle genes, SASP genes, and L1 elements, that have local changes in chromatin architecture in RS.

Methods

Cell Culture

LF1 human diploid fibroblasts were cultured in HAMS F-10 medium with 15% fetal bovine serum, penicillin, streptomycin, and glutamine. Cells for proliferating samples were harvested for Hi-C. Remaining cells were cultured to replicative exhaustion and maintained for 4-5 months after reaching senescence for senescent samples for Hi-C. Senescence was determined by staining for senescence-associated β-galactosidase [8].

Hi-C

Hi-C of proliferating and RS human diploid fibroblasts was done using the Arima Hi-C kit. The resulting data was aligned to the hg19 reference genome and processed using Juicer software tools [10]. Reads were filtered such that the mapping quality value MAPQ was greater than or equal to 30, and the RS matrix, which had more contacts than the proliferating matrix, was downsampled to match the proliferating. Heatmaps were generated with

a resolution of 3000 bp.

RNA-sequencing

Bulk RNA-sequencing was done using proliferating, quiescent, early RS, and late RS human diploid fibroblast cells. Reads were aligned to hg19, and differential expression analysis was done to compare the expression of each gene in each pair of conditions. Genes in the IFN pathway were found using IPA (QIAGEN Inc., https://www.qiagenbioinformatics.com/products/ingenuity- pathway-analysis).

Compartment Calls

Compartments were identified at a resolution of 1 megabase using the Juicer Tools eigenvector approach. The data is first broken down into bins of a set size. Then, Pearson's matrix is computed from the Hi-C matrix as the correlation matrix of the Observed/Expected values. The eigenvector is the first principal component of this matrix, and for each bin, the sign of the eigenvector indicates whether the bin is in the A compartment or the B compartment [10]. Whether the A or B compartment is associated with positive or negative eigenvectors is not constant, and because each chromosome is analyzed separately, is not consistent across chromosomes within a single Hi-C data set. Because compartment A is more gene-rich than compartment B, the compartments can be identified for each chromosome in each condition using the gene density of the negative and positive eigenvector regions for that chromosome and condition:

$$\text{gene density} = \frac{\text{\# of genes in regions with sign}}{\text{bp in regions with sign}}$$

Subcompartment Calls

Subcompartments were called for proliferating and senescent LF1 Hi-C data and for pre-existing data from another human diploid fibroblast strain, IMR90, based on inter-chromosomal contacts at 50 kilobase resolution using SLICE, an unpublished subcompartment caller from the Aiden lab.

IMR90 cells are more widely used than LF1 cells and have more available epigenetic data, which is used to label the IMR90 subcompartments as A1, A2, B1, B2, and B3. The similarity of subcompartment regions between IMR90 and proliferating LF1 cells (Fig. S2) allows the labeling of LF1 subcompartments using the IMR90 calls.

Subcompartments were quantified by finding the percentage of the genome covered by the regions in each subcompartment. Calls were compared between conditions and cell types by taking the regions of overlap between calls for each pair of subcompartments across conditions (A1 in proliferating and A1 in senescent, A1 in proliferating and A2 in senescent, and so on) and calculating what percentage of the genome is covered by the overlap.

TAD Calls

Three TAD caller softwares were used to call TADs for proliferating and senescent cells at 40 kilobase resolution: Juicer Tools' Arrowhead, Insulation Score (IS), and TADbit [10, 6, 21]. These use different computational approaches: arrowhead and IS use a linear score, and TADbit uses a statistical model [28]. TAD calls are difficult to compare quantitatively, as each set of TAD calls is a list of genomic regions which may or may not contain overlaps, gaps, or nesting. Two TADs identified by different might have a large amount of overlap but not share boundaries. Alternatively, a TAD from one set might be called as multiple sub-TADs by another caller, but both boundaries of the large TAD may still be

identified by both callers. Thus, there would be a tradeoff between amount of overlap and conservation of boundaries. The calls, then, are best assessed and compared on a local scale.

Loop Calls

Loops were called for the proliferating and senescent data using the MAPQ30 heatmap at a resolution of 40 kilobases with the Juicer Tools HiCCUPS algorithm [10]. Genes of interest, including SASP genes from [3] and cell cycle genes from [22], were then examined on the heatmap with expression data to investigate loop changes. Additionally, LINE1 elements which are intact and are activated in RS [3] were viewed and assessed for changes in loops. Cell cycle genes (Fig. S3), SASP genes (Fig. S4), and LINE1 elements (Fig. S5) with differentially expressed RNA and visually observable loop changes in the Hi-C data were noted, and regions were selected for further investigation based on the apparent strength of the loop changes.

Visualization

Heatmaps and relevant data, including genes, expression data, compartments, TADs, and loops, were visualized using Juicebox [9].

Results

Contact Distribution

We observe an increase in short-range contacts (< 20 kilobases) and a decrease in long-range contacts (> 20 kilobases) in RS compared to proliferating LF1 cells (Fig. 2). This

is consistent with previous work also using LF1 cells in deep RS [7]. However, early RS cells show the opposite pattern, with more long-range contacts and fewer short-range contacts in early senescence [27]. OIS models, which form SAHFs, also have an increase in long-range contacts in senescence [4, 20, 18]. This indicates first a difference between RS and OIS in the changes to long-range and short-range contact distribution, where OIS cells consistently have an increase in long-range contacts in senescence. Secondly, the decrease in long-range contacts in late RS seems to follow a period of increase in long-range contacts in early RS.

2a.

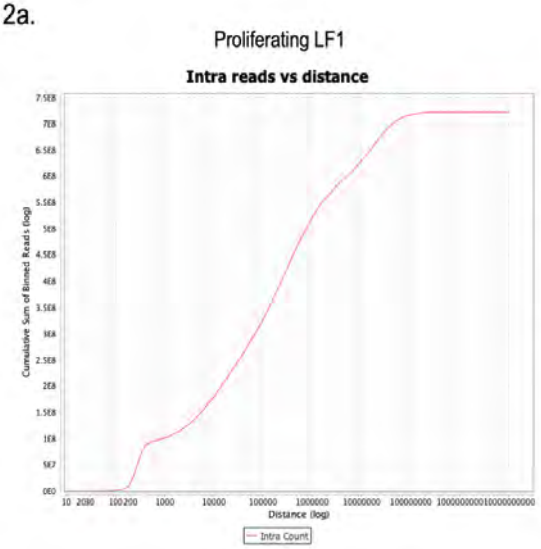

b.

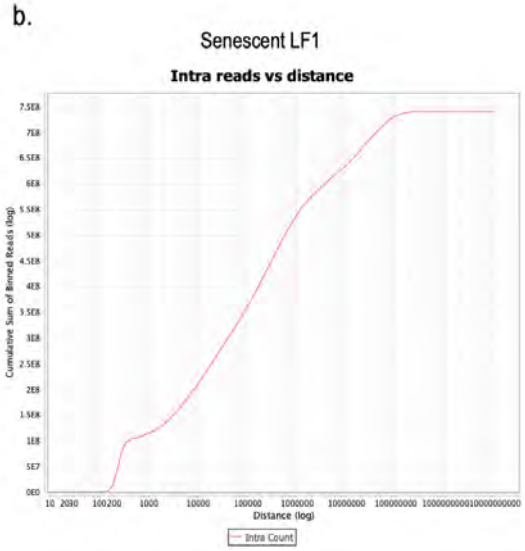

c.

Proliferating Contacts

Distance	Percent of Sequenced Reads	Percent of Unique Reads
Short Range (<20kb)	17.60	23.08
Long Range (>20kb)	40.15	52.63

d.

Senescent Contacts

Distance	Percent of Sequenced Reads	Percent of Unique Reads
Short Range (<20kb)	17.92	25.28
Long Range (>20kb)	34.10	48.12

Figure 2. Long range and short range contacts. There are slightly more short range contacts and fewer long range contacts in the RS Hi-C data than in the proliferating data, consistent with previous Hi-C of late RS cells.

Compartments

On a low resolution scale, compartment differences between proliferating and senescent cells can be observed. On the heatmap, visible large-scale differences can be seen as alterations to the checkerboard pattern associated with compartments, including a loss of distinct boundaries (Fig. 3). Quantitatively, 14.57% of compartment A from the proliferating calls becomes compartment B in the senescent calls, and 18.38% of compartment B from the proliferating calls becomes compartment A in the senescent calls (Fig. 3b). The gene density difference between the two compartments remains similar between proliferating and senescent conditions (Fig. 3c).

Although the majority of the compartments are conserved between proliferating and senescent conditions, the compartment changes are notable, as the compartment A to B change accounts for 211 megabases, and the compartment B to A change accounts for 295 megabases. Together, this is approximately 16% of the genome. Because compartment A is more euchromatic and compartment B is more heterochromatic [19], this large-scale change has implications for the expression of genes in regions that switch compartments between proliferating and senescent states.

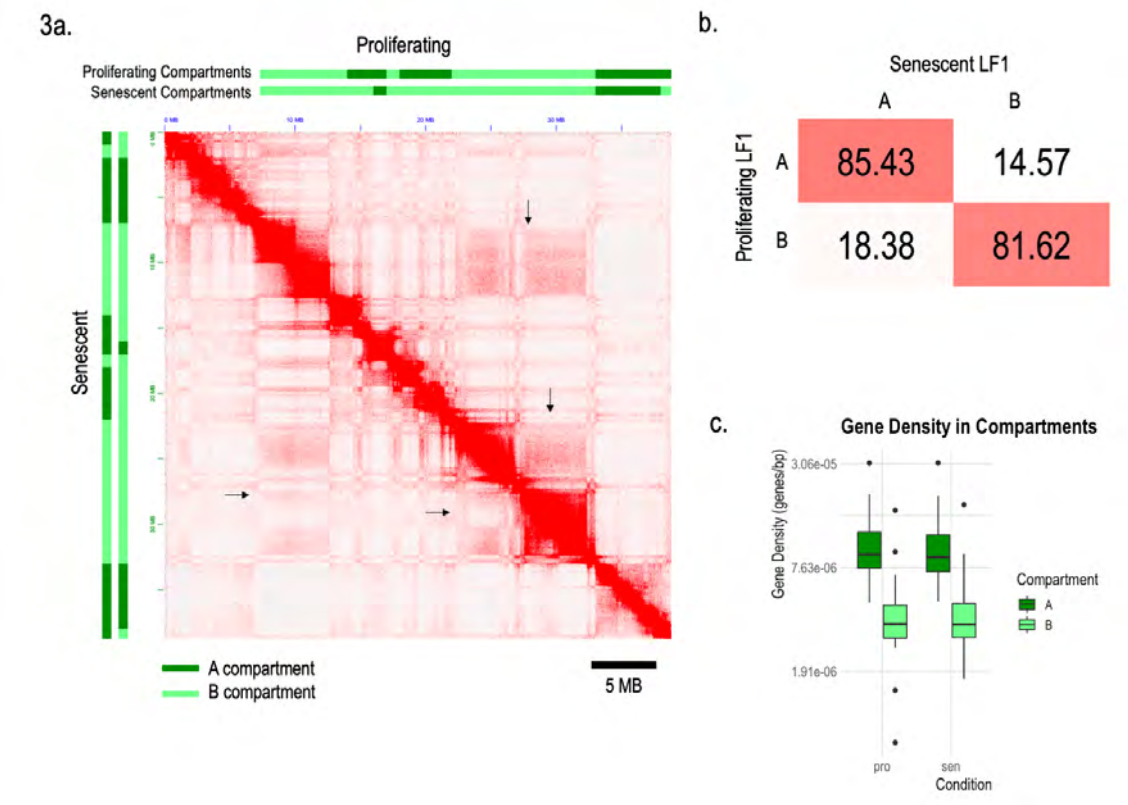

Figure 3. Genomic compartments can be identified from Hi-C data. Compartments can be seen from a low-resolution view of chromosomes as the checkerboard pattern of the heatmap. Shown here is the p arm of chromosome 9 from proliferating and senescent cells, with compartment calls shown ss tracks, where dark green is compartment A and light green is compartment B (a). Note the large-scale changes between the proliferating and senescent heatmaps, including the less distinct compartment boundaries in the senescent heatmap (indicated by arrows), particularly between 20 and 25 MB, where an A compartment region in proliferating cells becomes B compartment in senescent cells. With calls at 1 megabase resolution, the percent change in compartment calls is shown in transition matrix format, with the first row being the percent of proliferating compartment A that is in each compartment in RS (b). In both proliferating and senescent cells, gene density is higher in the A compartment than in the B compartment, which allows the labeling of compartments (c).

Subcompartments

Subcompartments were first identified only in the GM12878 lymphoblastoid cell line, as it was the only cell line with Hi-C data with enough reads to call subcompartments [19]. As more Hi-C data becomes available, subcompartments can be called and compared across cell types and conditions. To determine the number of subcompartments and the accuracy of the calls, interactions between genomic bins in each subcompartment are assessed through heatmaps. The existence of a distinct interaction profile for each subcompartment in the five-subcompartment model supports the presence five subcompartments in both proliferating and senescent LF1 cells and in proliferating IMR90 cells, a separate but similar human diploid fibroblast strain (Fig. S1), which correspond to the five main subcompartments identified in GM12878 cells: A1, A2, B1, B2, and B3 [19]. IMR90 cells were used because, while they are similar to LF1 cells, IMR90 cells are more widely used and have more available epigenetic data than LF1 cells. This epigenetic data is used to label the IMR90 subcompartments as A1, A2, B1, B2, and B3. The relatively similar subcompartment regions between IMR90 and proliferating LF1 cells (Fig. S2) then allows the labeling of LF1 subcompartments.

Quantification of each subcompartment (Fig. 4a) shows that the amount of the genome in subcompartment A1 increases in RS, and the amount of the genome in subcompartments B1 and B2 decreases in RS. The quantification of subcompartment changes between conditions (Fig. 4b) shows that the increase in A1 in RS comes most from regions that are B1 in proliferating cells, followed by A2. The B1 subcompartment regions that are lost in RS become mostly A1 and A2, and the lost B2 regions become mainly B1 and B3.

Subcompartments B1 and B2 are associated with facultative heterochromatin and pericentromeric chromatin, respectively [19]. The transition from B2 to B1 indicates pericentromeric chromatin interacting more with or becoming more similar to facultative hete-

rochromatin, ana the loss of subcompartment B1 to A subcompartments suggests the opening of facultative heterochromatin in RS. This loss of more heterochromatic subcompartments is consistent with previous studies which have found a loss of the B compartment in senescence, though in OIS rather than RS [16].

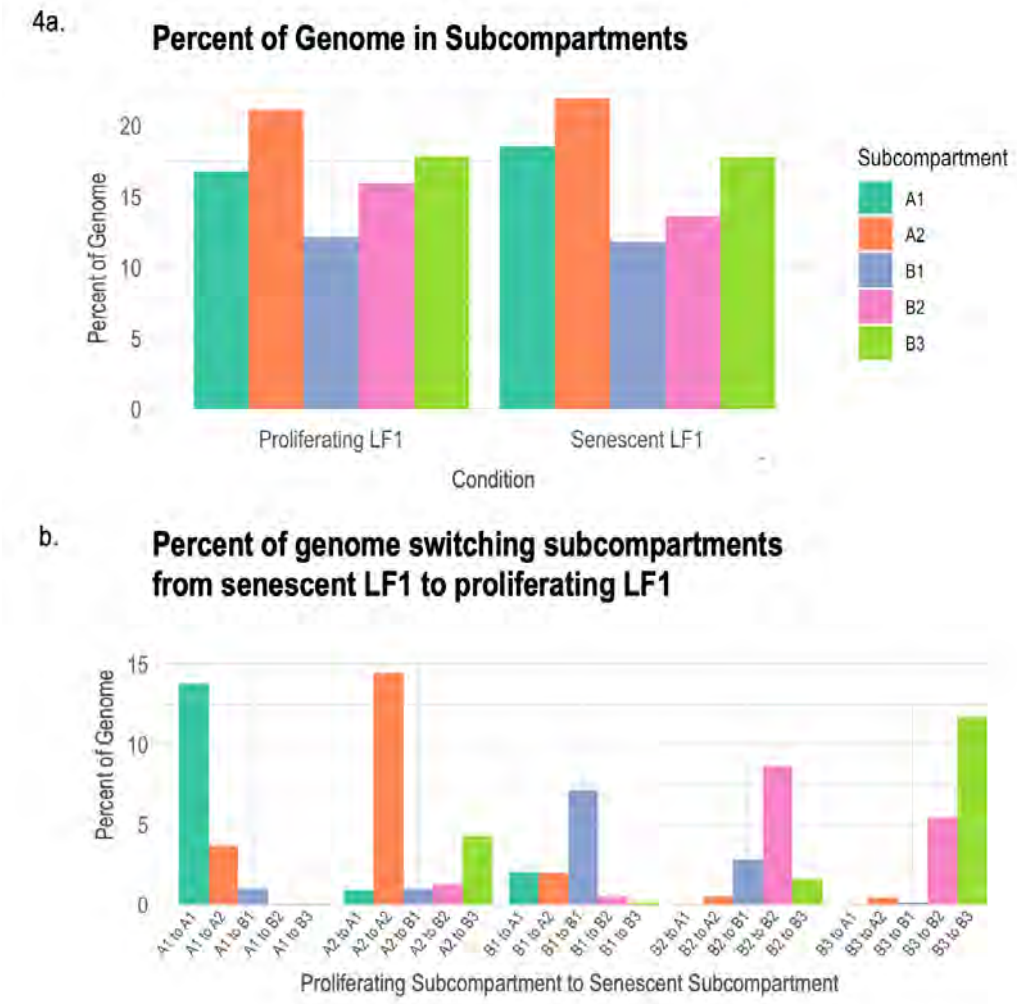

Figure 4. The five subcompartments were called using SLICE [unpublished, Aiden lab] at 50 kilobase resolution for proliferating and senescent LF1 cells. The percentage of the genome in each subcompartment is shown for both conditions (a). In (b), the percentage of the genome with each subcompartment transition between conditions is shown.

TADs

The inconsistency between TAD calling tools (Fig. 5d) and the lack of ground truth for the problem of TAD calling remain issues in the analysis of Hi-C data. Further, while each caller used identifies differences between proliferating and senescent LF1 TADs (Fig. 5a-c), it is difficult to quantitatively compare two lists of TADs. Different callers may or may not allow overlap or nesting of TADs or space between TADs, all of which complicate the issue. For example, TADbit calls non-overlapping TADs with no gaps (Fig. 5b) [28]. This would be the most straightforward case for comparing two conditions, since the comparison could be as simple as counting conserved boundary points. The Insulation Score method calls non-overlapping TADs, but there may be gaps between them (Fig. 5c) [28], which would require comparison of both start points and end points of TADs, rather than just the breaks between them as with TADbit. In the most complex case, Arrowhead allows overlap and gaps (Fig. 5a) [28], so that multiple TADs from the same list may share boundaries or some portion of their area, requiring more complex comparison methods than a sequential assessment of boundaries. Although models that include overlaps and gaps between TADs are the most difficult to analyze, the complexity of these models is most reflective of the organization of contacts on the Hi-C heatmaps and the actual hierarchical organization of chromatin. Thus, TADs remain best assessed on a local scale, by examining regions of particular interest.

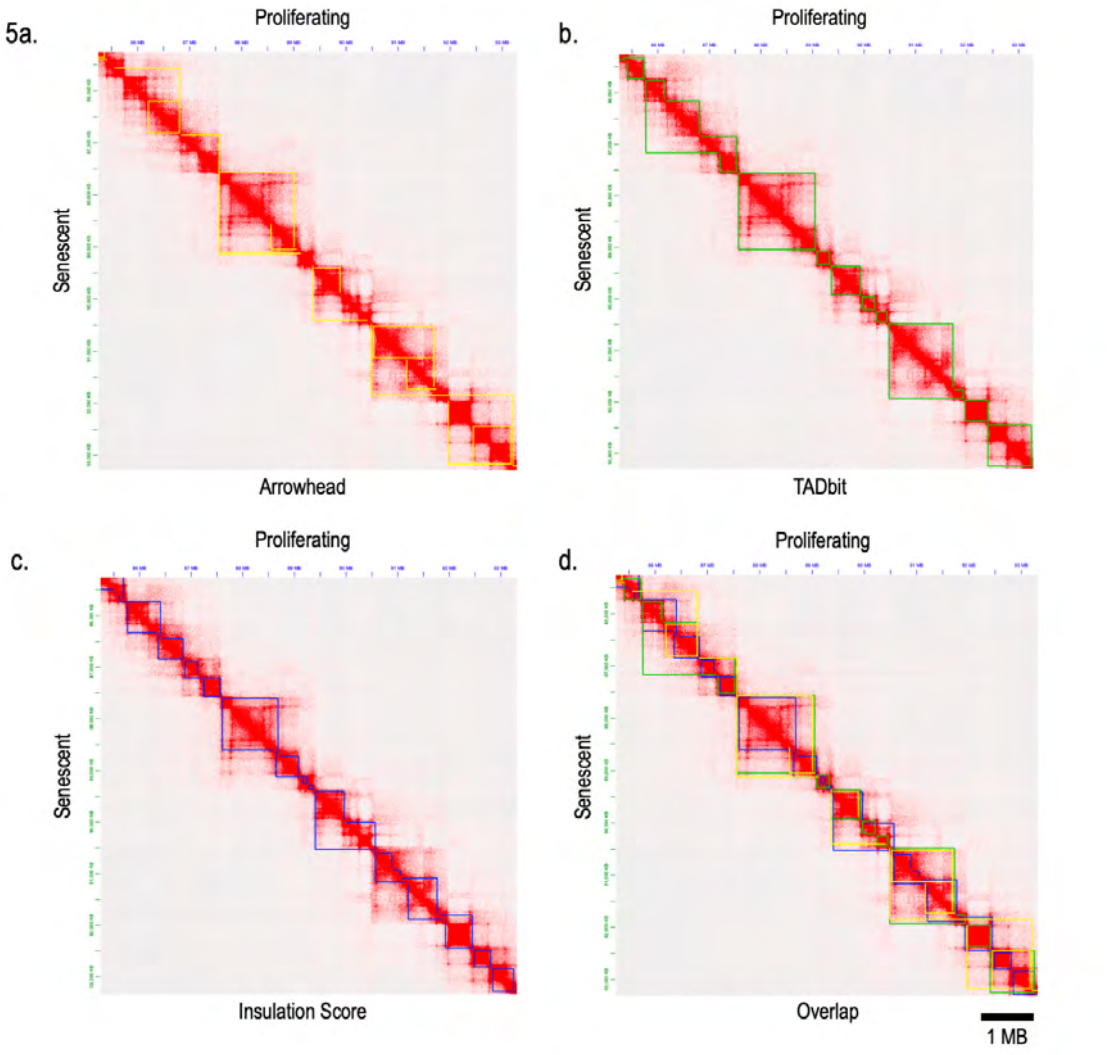

Figure 5. TAD callers are inconsistent when compared. Calls are shown at 10 kilobase resolution for a section of chromosome 1 for RS, with TADs called by arrowhead in yellow, TADs called by IS in blue, and TADs called by TADbit in green, with senescent below the diagonal and proliferating above the diagonal. Calls from different callers on the same condition tend not to agree (d). Calls from the same caller on different conditions are more similar (a-c).

Loops

Downregulated Genes

Among the genes previously known to be downregulated in CS are those involved in cell cycle processes. This includes genes required for DNA replication, such as MCM2, a component of the helicase complex [14], and genes required for mitosis, such as CENPE [13], the kinetochore-associated motor protein [26].

Changes in chromatin looping can be seen at the loci of multiple genes that are downregulated in RS, including MCM2 and CENPE (Fig. 6). A series of loops just upstream of MCM2 appears more distinct in RS, while the contacts in the domain immediately upstream appear slightly depleted in RS. In the domain immediately downstream, contacts appear enriched in RS compared to proliferating (Fig. 6a). Likewise, the loops immediately upstream and downstream of CENPE appear stronger in RS, and the domain immediately downstream has a more distinct boundary in RS compared to proliferating (Fig. 6b). The strengthening of loops in RS here coincides with a decrease in expression.

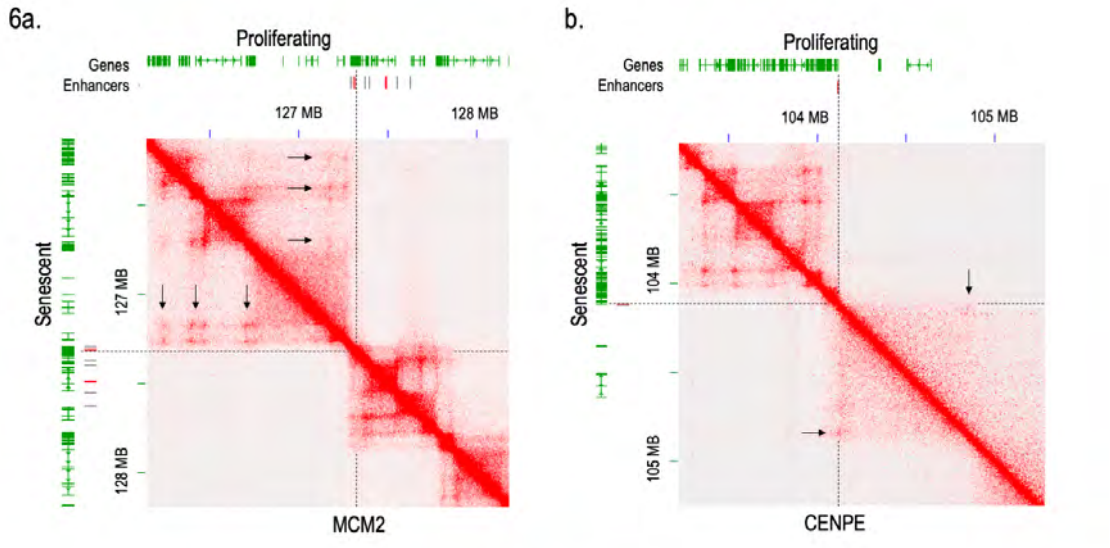

c.

Cell Cycle Gene RNA-seq Data

gene	log(fold change)	p-value	q-value
MCM2	-3.55644	5.00E-05	0.000260021
CENPE	-4.01466	5.00E-05	0.000260021

Figure 6. Loops and gene expression change at the MCM2 locus in RS. At 5 kilobase resolution, stronger looping can be seen on senescent heatmaps compared to proliferating at cell cycle genes including MCM2 (a) and CENPE (b). Dotted lines indicate genes of interest, and arrows point to loops. Enhancers with scores greater than 5 for the genes of interest are shown as a track [12]. MCM2 and CENPE are expressed at lower levels in RS than in proliferating cells (c).

Upregulated Genes

Genes that are differentially upregulated in senescence include SASP genes such as Insulin-like growth factor-1 (IGF1) and interferons (IFNs) [5, 2, 3]. IGF1 signaling is involved in growth and proliferation, but can also lead to increased p53 activity, which, in turn, promotes senescence [5, 25]. The chromosome 9 IFN cluster is also highly expressed in late

senescence in response to L1 activation [3].

At the IFN cluster, an increase in looping can be observed in RS (Fig. 7a). While the RNA-seq data does not detect sufficient mRNA for the genes in this cluster (Fig. 7d), several genes downstream in the IFN signaling pathway are significantly upregulated, indicating increased IFN activity (Fig. 7c). Similarly, an increase in loop definition can be observed around the IGF1 locus (Fig. 7b), and IGF1 is significantly upregulated in late RS (Fig. 7d). In these cases, an increase in loop presence coincides with an increase in expression.

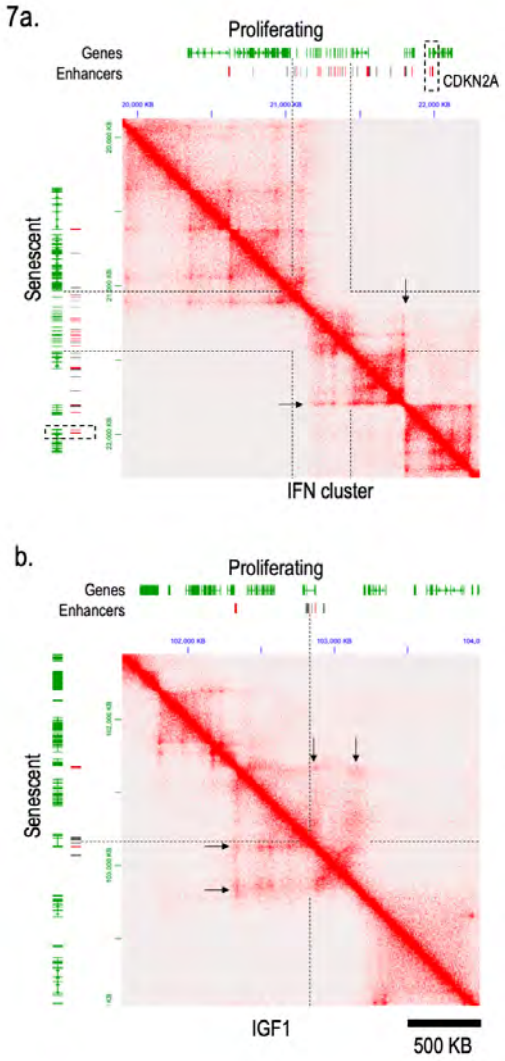

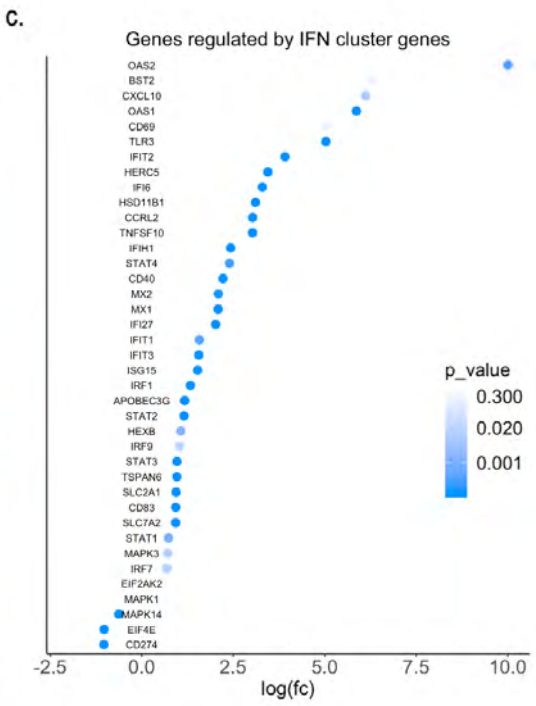

d.

SASP Gene RNA-seq Data

gene	log(fold change)	p-value	q-value
IGF1	3.74277	0.00225	0.00814762
IFNB1	0	1	1
IFNW1	0	1	1
IFNE	3.12347	0.0002	0.000937149
IFNA4	0	1	1

Figure 7. Loops and gene expression change at SASP genes in RS. At 5 kilobase resolution, stronger looping can be seen on senescent heatmaps compared to proliferating at SASP genes including the IFN cluster (a) and IGF1 (b). Dotted lines indicate genes of interest, and arrows point to loops. CDKN2A, a senescence marker, is also labeled. Enhancers with scores greater than 5 for the genes of interest are shown as a track [12]. IGF1 (d) and multiple genes regulated by genes in the IFN cluster (c) are signficantly more highly expressed in late RS, compared to proliferating cells.

LINE-1 elements

L1 transcription is activated in RS, and the specific elements that are activated have previously been identified [3]. Specifically, intact L1HS elements that are active in RS were investigated alongside the Hi-C data, revealing that at some of these elements, there are clearly visible changes in loop and TAD organization (Fig. 8). This has implications for the means by which L1 elements are activated and for the involvement of three-dimensional organization in the activation of repressed chromatin.

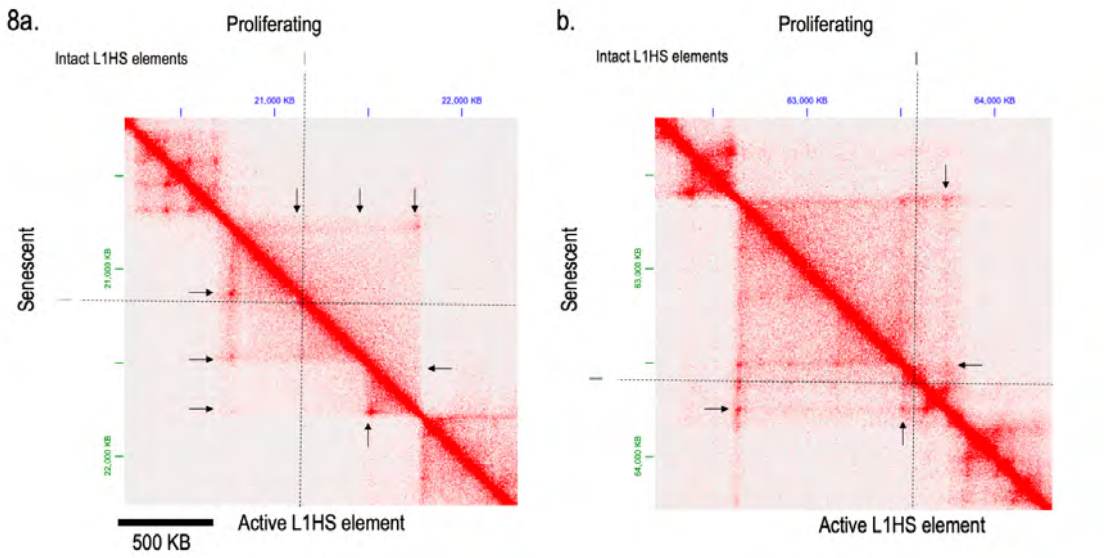

Figure 8. Loops change at LINE-1 elements. At 5 kilobase resolution, loop and TAD changes can be seen at some LINE1 elements that are active in CS [3]. Dotted lines indicate elements of interest, and arrows point to loops. Intact L1 elements are shown as a track.

Discussion

High-resolution Hi-C reveals differences in chromatin organization between proliferating and senescent cells. On the level of compartments, the findings here add to what is already know about the changes to euchromatin and heterochromatin in RS. Subcompartments have not previously been called for RS cells, as a large number of reads is required to do so. The changes in subcompartments supports the previous observation that heterochromatin is lost in RS. Future studies may confirm the identities of these subcompartments using histone markers and other identifying features.

While TAD calling remains an issue, it does present a problem for which machine learning may be useful. However, with the current tools available, local inspection of TADs and loops can identify regions of interest for future study of the associations between higher order chromatin structure and gene expression. In this case, SASP genes, cell cycle genes, and L1 elements all present targets for further investigation of organization and expression in senescence.

The regions of interest identified suggest a role for chromatin reorganization in senescence as a potential contributor to the changes seen in gene expression. Alternatively, changes in gene expression resulting from senescence may drive the opening of chromatin in some regions. Further studies using promoter-capture Hi-C could indicate whether the changes in looping correspond to changes in promoter-enhancer contacts at particular genes in ways that could affect gene expression levels.

Some of the most distinct small-scale changes in RS are observed at L1 elements that are known to be expressed in RS. This presents the question of whether the changes to the organization of chromatin, and specifically the loss of heterochromatin, that are characteristic of CS lead to the expression of L1 elements and, eventually, to IFN overexpression in late senescence. While there are several open questions remaining about chromatin organization and activity in senescence, a high-resolution Hi-C map provides a framework for investigating these questions and for discovering new questions.

References

[1] Ferhat Ay and William S. Noble. Analysis methods for studying the 3d architecture of the genome. *Genome Biology*, 16, 2015.

[2] Nathan Basisty, Abhijit Kale, Ok Hee Jeon, Chisaka Kuehnemann, Therese Payne, Chirag Rao, Anja Holtz, Samah Shah, Vagisha Sharma, Luigi Ferrucci, Judith Campisi, and Birgit Schilling. A proteomic atlas of senescence-associated secretomes for aging biomarker development. *PLOS Biology*, 18(1):1–26, 01 2020.

[3] Marco De Cecco, Takahiro Ito, Anna P. Petrashen, Amy E. Elias, Nicholas J. Skvir, Steven W. Criscione, Alberto Caligiana, Greta Brocculi, Emily M. Adney, Jef D. Boeke, Oanh Le, Christian Beauséjour, Jayakrishna Ambati, Kameshwari Ambati, Matthew Simon, Andrei Seluanov, Vera Gorbunova, P. Eline Slagboom, Stephen L. Helfand, Nicola Neretti, , and John M. Sedivy. Line-1 derepression in senescent cells triggers interferon and inflammaging. *Nature*, 566(7742):73–78, 2019.

[4] Tamir Chandra, Philip Andrew Ewels, Stefan Schoenfelder, Mayra Furlan-Magaril, Steven William Wingett, Kristina Kirschner, Jean-Yves Thuret, Simon Andrews, Peter Fraser, , and Wolf Reik. Global reorganization of the nuclear landscape in senescent cells. *Cell Reports*, 10(4):471–483, 2015.

[5] Jean-Philippe Coppé, Christopher K Patil, Francis Rodier, Yu Sun, Denise P Muñoz, Joshua Goldstein, Peter S Nelson, Pierre-Yves Desprez, and Judith Campisi. Senescence-associated secretory phenotypes reveal cell-nonautonomous functions of oncogenic ras and the p53 tumor suppressor. *PLOS Biology*, 6(12):1–1, 12 2008.

[6] Emily Crane, Qian Bian, Rachel Patton McCord, Bryan R Lajoie, Bayly S Wheeler, Edward J Ralston, Satoru Uzawa, Job Dekker, and Barbara J Meyer. Condensin-

driven remodelling of x chromosome topology during dosage compensation. *Nature*, 523(7559):240–244, 2015.

[7] Steven W. Criscione, Marco De Cecco, Benjamin Siranosian, Yue Zhang, Jill A. Kreiling, John M. Sedivy, and Nicola Neretti. Reorganization of chromosome architecture in replicative cellular senescence. *Science Advances*, 2(2), 2016.

[8] G P Dimri, X Lee, G Basile, M Acosta, G Scott, C Roskelley, E E Medrano, M Linskens, I Rubelj, and O Pereira-Smith. A biomarker that identifies senescent human cells in culture and in aging skin in vivo. *Proceedings of the National Academy of Sciences*, 92(20):9363–9367, 1995.

[9] Neva C. Durand, James T. Robinson, Muhammad S. Shamim, Ido Machol, Jill P. Mesirov, Eric S. Lander, and Erez Lieberman Aiden. Juicebox provides a visualization system for hi-c contact maps with unlimited zoom. *Cell Systems*, 3(1), 2016.

[10] Neva C. Durand, Muhammad S. Shamim, Ido Machol, Suhas S. P. Rao, Miriam H. Huntley, Eric S. Lander, and Erez Lieberman Aiden. Juicer provides a one-click system for analyzing loop-resolution hi-c experiments. *Cell Systems*, 3(1), 2016.

[11] Shane A. Evans, Jeremy Horrell, and Nicola Neretti. The three-dimensional organization of the genome in cellular senescence and age-associated diseases. *Seminars in Cell & Developmental Biology*, 90:154 – 160, 2019. 3D Genome and Diseases.

[12] Simon Fishilevich, Ron Nudel, Noa Rappaport, Rotem Hadar, Inbar Plaschkes, Tsippi Iny Stein, Naomi Rosen, Asher Kohn, Michal Twik, Marilyn Safran, Doron Lancet, and Dana Cohen. GeneHancer: genome-wide integration of enhancers and target genes in GeneCards. *Database*, 2017, 04 2017. bax028.

[13] Valentina Gambino, Giulia De Michele, Oriella Venezia, Pierluigi Migliaccio, Valentina Dall'Olio, Loris Bernard, Simone Paolo Minardi, Maria Agnese Della Fazia, Daniela Bartoli, Giuseppe Servillo, Myriam Alcalay, Lucilla Luzi, Marco Giorgio, Heidi Scrable, Pier Giuseppe Pelicci, and Enrica Migliaccio. Oxidative stress activates a specific p53 transcriptional response that regulates cellular senescence and aging. *Aging Cell*, 12(3):435–445, 2013.

[14] Hideki Harada, Hiroshi Nakagawa, Munenori Takaoka, James Lee, Meenhard Herlyn, J. Allan Diehl, and Anil K. Rustgi. Cleavage of mcm2 licensing protein fosters senescence in human keratinocytes. *Cell Cycle*, 7(22):3534–3538, 2008. PMID: 19001876.

[15] L. Hayflick and P.S. Moorhead. The serial cultivation of human diploid cell strains. *Experimental Cell Research*, 25(3):585 – 621, 1961.

[16] Osamu Iwasaki, Hideki Tanizawa, Kyoung-Dong Kim, Andrew Kossenkov, Timothy Nacarelli, Sanki Tashiro, Sonali Majumdar, Louise C. Showe, Rugang Zhang, and Ken ichi Noma. Involvement of condensin in cellular senescence through gene regulation and compartmental reorganization. *Nature Communications*, 10(5688), 2019.

[17] Masashi Narita, Sabrina Nuñez, Edith Heard, Masako Narita, Athena W. Lin, Stephen A. Hearn, David L. Spector, Gregory J. Hannon, and Scott W. Lowe. Rb-mediated heterochromatin formation and silencing of e2f target genes during cellular senescence. *Cell*, 113(6):703 – 716, 2003.

[18] Ioana Olan, Aled J. Parry, Stefan Schoenfelder, Masako Narita, Yoko Ito, Adelyne S. L. Chan, Guy St.C. Slater, Dóra Bihary, Masashige Bando, Katsuhiko Shirahige, Hiroshi Kimura, Shamith A. Samarajiwa, Peter Fraser, and Masashi Narita. Transcription-dependent cohesin repositioning rewires chromatin loops in cellular senescence. *Nature Communications*, 11(6049), 2020.

[19] Suhas S.P. Rao, Miriam H. Huntley, Neva C. Durand, Elena K. Stamenova, Ivan D. Bochkov, James T. Robinson, Adrian L. Sanborn, Ido Machol, Arina D. Omer, Eric S. Lander, and Erez Lieberman Aiden. A 3d map of the human genome at kilobase resolution reveals principles of chromatin looping. *Cell*, 159(7):1665 – 1680, 2014.

[20] Satish Sati, Boyan Bonev, Quentin Szabo, Daniel Jost, Paul Bensadoun, Francois Serra, Vincent Loubiere, Giorgio Lucio Papadopoulos, Juan-Carlos Rivera-Mulia, Lauriane Fritsch, Pauline Bouret, David Castillo, Josep Ll. Gelpi, Modesto Orozco, Cedric Vaillant, Franck Pellestor, Frederic Bantignies, Marc A. Marti-Renom, David M. Gilbert, Jean-Marc Lemaitre, , and Giacomo Cavalli. 4d genome rewiring during oncogene- induced and replicative senescence. *Molecular Cell*, 78:522 – 538, 2020.

[21] François Serra, Davide Baù, Mike Goodstadt, David Castillo, Guillaume J. Filion, and Marc A. Marti-Renom. Automatic analysis and 3d-modelling of hi-c data using tadbit reveals structural features of the fly chromatin colors. *PLOS Computational Biology*, 13(7), 2017.

[22] Tim Stuart, Andrew Butler, Paul Hoffman, Christoph Hafemeister, Efthymia Papalexi, William M Mauck III, Yuhan Hao, Marlon Stoeckius, Peter Smibert, and Rahul Satija. Comprehensive integration of single-cell data. *Cell*, 177:1888–1902, 2019.

[23] Luyang Sun, Ruofan Yu, and Weiwei Dang. Chromatin architectural changes during cellular senescence and aging. *Genes*, 9(4), 2018.

[24] Eric C. Swanson, Benjamin Manning, Hong Zhang, and Jeanne B. Lawrence. Higher-order unfolding of satellite heterochromatin is a consistent and early event in cell senescence. *Journal of Cell Biology*, 203(6):929–942, 12 2013.

[25] Duc Tran, Johann Bergholz, Haibo Zhang, Hanbing He, Yang Wang, Yujun Zhang, Qintong Li, James L. Kirkland, and Zhi-Xiong Xiao. Insulin-like growth factor-1 regulates the sirt1-p53 pathway in cellular senescence. *Aging Cell*, 13(4):669–678, 2014.

[26] Kenneth W Wood, Roman Sakowicz, Lawrence S.B Goldstein, and Don W Cleveland. Cenp-e is a plus end–directed kinetochore motor required for metaphase chromosome alignment. *Cell*, 91(3):357–366, 1997.

[27] Anne Zirkel, Milos Nikolic, Konstantinos Sofiadis, Jan-Philipp Mallm, Chris A. Brackley, Henrike Gothe, Oliver Drechsel, Christian Becker, Janine Altmüller, Natasa Josipovic, Theodore Georgomanolis, Lilija Brant, Julia Franzen, Mirjam Koker, Eduardo G. Gusmao, Ivan G. Costa, Roland T. Ullrich, Wolfgang Wagner, Vassilis Roukos, Peter Nürnberg, Davide Marenduzzo, Karsten Rippe, and Argyris Papantonis. Hmgb2 loss upon senescence entry disrupts genomic organization and induces ctcf clustering across cell types. *Molecular Cell*, 70(4):730 – 744.e6, 2018.

[28] Marie Zufferey, Daniele Tavernari, Elisa Oricchio, and Giovanni Ciriello. Comparison of computational methods for the identification of topologically associating domains. *Genome Biology*, 19(217), 2018.

Supplemental Figures

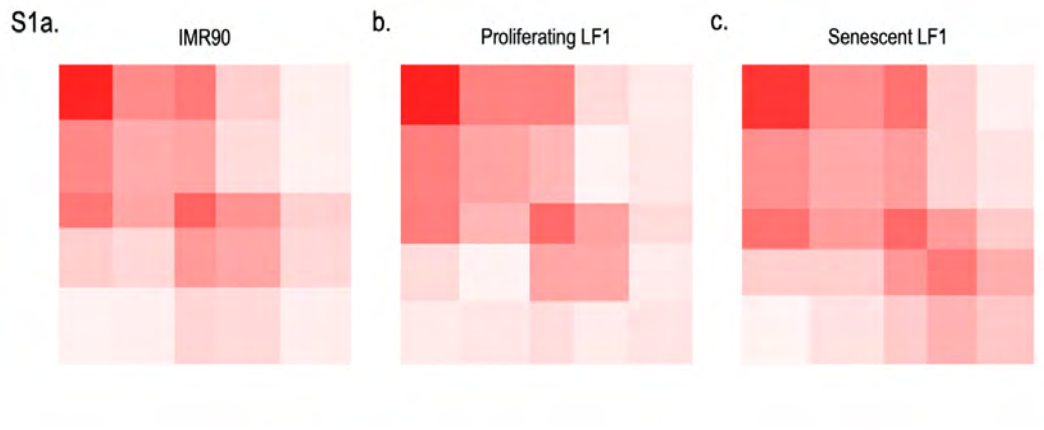

Figure S1. There are five distinct subcompartments for proliferating and senescent LF1 cells and for proliferating IMR90 cells. Heatmaps are generated using the interactions of each pair of subcompartment to assess whether each subcompartment called is distinct. Interactions between regions of each subcompartment have distinct profiles under a five-subcompartment model (a-c).

S2a.

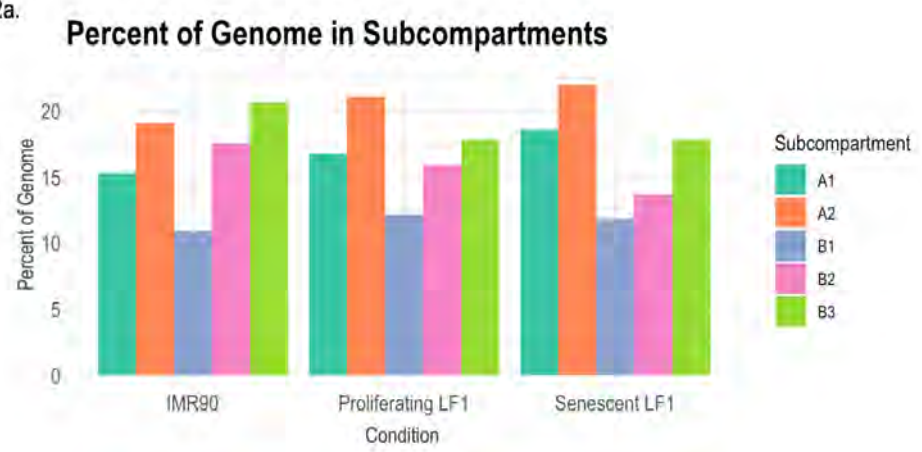
Percent of Genome in Subcompartments
Percent of Genome
20
15
10
5
0
IMR90
Proliferating LF1
Senescent LF1
Condition
Subcompartment
A1
A2
B1
B2
B3

b.

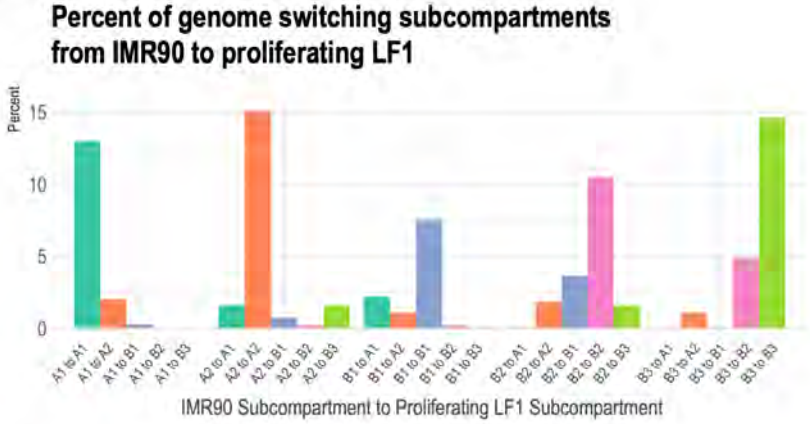
Percent of genome switching subcompartments from IMR90 to proliferating LF1
Percent
15
10
5
0
IMR90 Subcompartment to Proliferating LF1 Subcompartment

c.

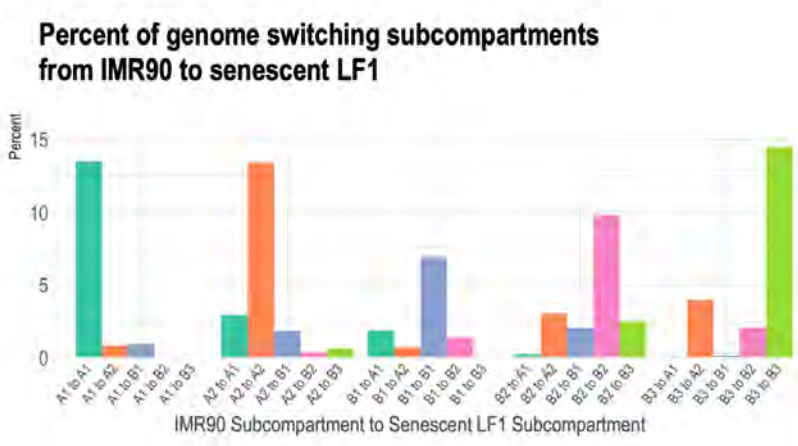
Percent of genome switching subcompartments from IMR90 to senescent LF1
Percent
15
10
5
0
IMR90 Subcompartment to Senescent LF1 Subcompartment

Figure S2. The five subcompartments were called using SLICE [unpublished, Aiden lab] at 50 kilobase resolution for proliferating and senescent LF1 cells and for IMR90 cells. The percentage of the genome in each subcompartment is shown for each cell type/condition (a). In (b) and (c), the percentage of the genome with each subcompartment transition between cell types is shown. The similarity between the calls for proliferating LF1 and IMR90 (b), for which there is more epigenetic data available, allows the labeling of LF1 subcompartments using similarity to the more easilt labeled IMR90 subcompartments.

S3a.

Cell Cycle Genes

Gene	Loop Change	Expression Change	Gene	Loop Change	Expression Change	Gene	Loop Change	Expression Change
RPA2	yes	no	GAS2L3	yes	yes	HJURP	yes	no
CLSPN	yes	yes	UNG	yes	yes	PCNA	yes	yes
CDCA8	yes	no	CKAP2	yes	no	TPX2	yes	yes
CDC20	yes	no	G2E3	yes	no	UBE2C	yes	yes
KIF2C	no	yes	DLGAP5	yes	no	AURKA	yes	yes
NASP	yes	no	UBR7	yes	yes	CHAF1B	yes	yes
USP1	yes	yes	RAD51	yes	no	CDC45	yes	no
PSRC1	yes	no	NUSAP1	yes	no	MCM5	yes	yes
ANP32E	yes	no	WDR76	yes	no	RANGAP1	yes	no
CKS1B	yes	yes	CCNB2	yes	yes	GTSE1	yes	yes
NUF2	yes	yes	TIPIN	yes	yes	SMC4	yes	yes
NEK2	yes	yes	KIF23	yes	yes	ECT2	yes	yes
DTL	yes	yes	BLM	yes	yes	SLBP	yes	no
CENPF	yes	yes	CTCF	yes	yes	TACC3	yes	no
LBR	yes	no	GINS2	yes	no	CENPE	yes	yes
EXO1	yes	yes	FAM64A	yes	no	HMGB2	yes	yes
CDK1	yes	no	AURKB	yes	no	CDC25C	yes	yes
KIF20B	yes	yes	CDC6	yes	yes	HMMR	yes	no
KIF11	yes	yes	TOP2A	yes	yes	GMNN	yes	no
HELLS	yes	no	BRIP1	yes	yes	TTK	yes	yes
MKI67	yes	no	HN1	yes	no	CASP8AP2	yes	yes
RRM1	yes	no	BIRC5	yes	no	ANLN	yes	yes
E2F8	yes	yes	TYMS	yes	no	RFC2	yes	yes
CKAP5	yes	yes	NDC80	yes	yes	CDCA2	yes	yes
FEN1	yes	no	UHRF1	yes	no	MCM4	yes	no
POLD3	yes	yes	RRM2	yes	yes	CCNE2	yes	yes
RAD51AP1	yes	no	CENPA	yes	yes	DSCC1	yes	yes
NCAPD2	yes	no	MSH2	yes	yes	ATAD2	yes	yes
CDCA3	yes	no	BUB1	yes	no	CKS2	yes	yes
CBX5	yes	no	CKAP2L	yes	no	TUBB4B	yes	no
PRIM1	yes	yes	MCM6	yes	yes	POLA1	yes	yes
TMPO	yes	yes	CDCA7	yes	no			

b. Cell Cycle Gene Loop and Expression Changes

Loop Changes	Expression changes	Number
yes	yes	53
yes	no	41
no	yes	1
no	no	0
	total:	95

Figure S3. Cell cycle gene loop and expression changes. For each gene in the list of cell cycle genes from [22], visible loop changes and RNA-seq significance were noted (a). Of the 53 with both loop changes and significant expression changes (b), two with some of the most clear changes were chosen for further investigation (Fig. 6).

S4a.

SASP genes

Gene	Loop Change	Expression Change	Gene	Loop Change	Expression Change
ISG15	no	yes	IL15	no	yes
TNFRSF1B	no	yes	VEGFC	no	yes
IFI6	no	yes	IRF1	yes	no
JUN	no	no	ITGA2	yes	yes
JAK1	yes	yes	IL6ST	yes	yes
CSF1	yes	yes	CSF2	no	yes
NGF	yes	yes	IRF1	no	yes
ADAR	yes	no	IL13	no	no
MNDA	no	no	TMEM173	no	no
IFI16	no	no	BMP6	yes	yes
CD55	yes	no	VEGFA	no	yes
EIF2AK2	no	no	IGF2R	yes	yes
PIGF	yes	no	IL6	no	yes
MAL	no	no	INHBA	no	yes
IL1A	no	yes	IGFBP1	yes	yes
IL1B	no	yes	EGFR	no	yes
IFIH1	yes	yes	CCL26	no	no
STAT1	yes	yes	HGF	yes	yes
IGFBP2	no	yes	SERPINE1	no	yes
INHA	no	no	CAV1	no	no
CCL20	yes	yes	MET	no	no
MYD88	yes	no	WNT2	yes	no
TNFSF10	no	yes	IRF5	no	no
CXCL6	yes	yes	TNFRSF10C	no	yes
CXCL1	yes	yes	IL7	no	no
CXCL5	yes	no	GEM	no	yes
CXCL3	yes	no	TNFRSF11B	yes	yes
CXCL2	yes	yes	JAK2	no	no
EREG	no	no	IFNB1	yes	no
AREG	no	yes	IFNW1	yes	no
CXCL10	no	no	IFNA4	yes	no
CXCL11	no	no	IFNA2	yes	no
FGF2	yes	yes	IFNA1	yes	no

SASP genes

Gene	Loop Change	Expression Change	Gene	Loop Change	Expression Change
IFNE	yes	yes	ISG20	no	yes
DDX58	no	yes	IQGAP1	yes	yes
PTGES	no	yes	MMP2	yes	yes
CXCL12	no	yes	NOS2	yes	no
FAS	no	yes	CCL2	yes	yes
IFIT2	no	yes	CCL7	yes	no
IFIT3	no	yes	CCL13	yes	no
IFIT1	no	yes	CCL1	yes	no
IFITM2	no	no	CCL3	no	no
IFITM1	no	yes	CSF3	yes	no
IFITM3	no	yes	STAT3	no	yes
IRF7	no	yes	TIMP2	yes	yes
MMP7	no	no	SERPINB2	yes	yes
MMP10	no	no	CCL25	no	no
MMP1	no	yes	ICAM1	yes	yes
MMP3	no	no	ICAM3	yes	no
MMP12	no	yes	BST2	no	no
MMP13	no	no	IFI30	no	yes
CASP1	yes	yes	GDF15	no	yes
CD9	no	yes	GMFG	no	no
TNFRSF1A	no	no	AXL	yes	yes
IGFBP6	yes	yes	TGFB1	yes	no
STAT2	no	yes	PLAUR	no	no
IGF1	yes	yes	IRF3	no	no
OAS1	yes	yes	BMP2	yes	yes
OAS2	yes	yes	MMP9	yes	no
ANG	no	yes	IFNAR2	yes	no
MMP14	yes	yes	IFNAR1	yes	yes
IRF9	no	yes	ETS2	yes	yes
RPS6KA5	no	no	MX2	yes	yes
IFI27	no	yes	MX1	yes	yes
ITPKA	no	no	MIF	no	no
FGF7	no	no	CSF2RB	yes	no

b.

SASP Gene Loop and Expression Changes

Loop Changes	Expression changes	Number
yes	yes	36
yes	no	22
no	yes	39
no	no	33
	total:	132

Figure S4. SASP gene loop and expression changes. For each gene in the list from [3], visible loop changes and RNA-seq significance were noted (a). Of the 36 with both loop changes and significant expression changes (b), two with some of the most clear changes were chosen for further investigation (Fig. 7).

S5.

Active L1 Elements

Chromosome	Start	End	Loop Change
1	119393972	119399998	yes
1	180834934	180840989	no
2	167843960	167849996	yes
3	158812139	158818184	yes
4	21160012	21166043	yes
5	103853286	103859315	no
6	2416992	2423021	yes
7	49718853	49724885	yes
8	129464221	129470252	yes
10	100541683	100547715	yes
14	63582411	63588440	yes
14	71013005	71019056	yes
15	71020991	71026498	no
16	9677334	9683374	yes
17	9518301	9524341	no
17	64592198	64598214	no
X	11952389	11958615	no
X	47642056	47648085	no
X	154744664	154750693	no

Figure S5. L1 loop and changes. For each intact L1 element identified as active [3], visible loop changes were noted. Images were included as examples in Figure 8 for the chromosome 4 element and for the element at 63.5 MB on chromosome 14.